The Effect of Ray Curvature on Lloyd's Mirror Fringe Estimates and Source Localisation

P.R. Lewis

DEPARTMENT OF DEFENCE
DEFENCE SCIENCE AND TECHNOLOGY ORGANISATION

The Effect of Ray Curvature on Lloyd's Mirror Fringe Estimates and Source Localisation

P.R. Lewis

Maritime Operations Division
Aeronautical and Maritime Research Laboratory

DSTO-TR-0064

ABSTRACT

A knowledge of the interference between direct, surface and bottom refelected rays emanating from a moving underwater source can be used to determine the source-detector relative positions. Using simple ray tracing, the frequency-time interference patterns for a broadband frequency source arising when the propagating medium has a piecewise linear sound speed profile are considered, and are compared with those for a constant sound speed. It is found that even small deviations from a constant sound speed can lead to a noticeably different interference fringe placement and shape, and consequently to the inferred source-detector geometry. Further, comparisons of model calculations to experimentally observed fringe systems demonstrate the inadequacy of the constant sound speed model, whereas the use of the simple segmented profile is capable of replicating the observed patterns.

DEPARTMENT OF DEFENCE

DEFENCE SCIENCE AND TECHNOLOGY ORGANISATION

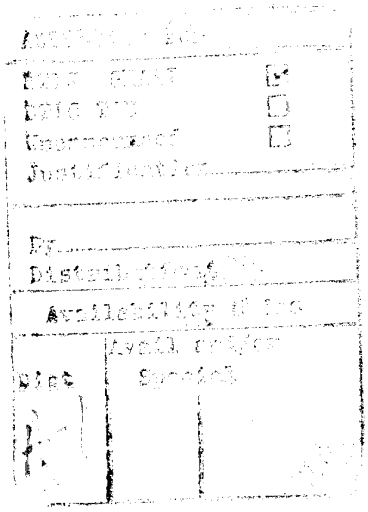

Published by

DSTO Aeronautical and Maritime Research Laboratory
GPO Box 4331
Melbourne Victoria 3001

Telephone: (03) 626 8111
Fax: (03) 626 8999

AR No. 008-927
September 1994

APPROVED FOR PUBLIC RELEASE

The Effect of Ray Curvature on Lloyd's Mirror Fringe Estimates and Source Localisation

EXECUTIVE SUMMARY

This report considers the effect a realistic sound speed profile, or variation of the sound speed with water depth, can have on the passive detection and range estimation of a source. Because of reflections from the sea surface or floor, the sound measured at a hydrophone can be the result of wave interference between the directly transmitted and a reflected sound wave, each of which is emitted from the source (the Lloyd's mirror effect). This interference will cause the sound intensity measured at the hydrophone to be modified depending on the source position and the frequency of the sound. Hence for a moving source, the measured sound intensity will fluctuate with time and the frequency. Further, for fixed source and hydrophone positions the variation will be dependent on the way in which the sound propagates through the water, or equivalently, the way the speed of sound varies with depth (and location). Depending on the structure of the sound speed profile, the variation may be important at a given distance, whilst any effects arising from the structure of the sound speed profile will become more evident with increasing separation of the source and hydrophone. The information inherent in these sound intensity variations allows an accurate estimation of the source range, or position relative to the hydrophone, but is based on an assumed model of sound propagation. It is important then to consider whether the simple model of a constant sound speed is adequate when extracting this information.

Predictions based on a variable, but still simple, sound speed profile are presented. Firstly, a phenomenological appraisal of the differences that can arise by the choice of either the constant or the simple variable sound speed models is made. This is based on several realistic sound speed profiles appropriate for the Australian costal region. Significant effects can be obtained, depending on the size of the differences between these two types of profile, and are found to be present for even small ranges ($\approx 0.5 - 1$ km). Thus, the type of assumed model can realistically be expected to affect the extracted source positional information even for passive detection, which is generally only of short range.

We then compare some true data and the predictions based on each of the two sound speed profile models. These data show a strong Lloyd's mirror effect. The comparisons indicate that a variable sound speed profile is necessary in order that a suitable description of some of the data is obtained: the constant sound speed profile is not capable of correctly reproducing these data. We also find that even when either model provides an adequate description, the estimated source positions differ by a noticeable amount, contrary to the expectation that the estimated source positions should be similar.

In conclusion, the Lloyd's mirror effect can be used to provide an accurate estimate of the source position relative to the hydrophone, but this estimate is dependent on the assumed model of sound propagation. A variable sound speed profile can make a significant difference, and is necessary in describing some of the experimental data. Therefore, it is important that the suitability of the underlying model of propagation be ascertained, and in particular the suitability of the constant sound speed model, before the deduced source position is accepted.

Author

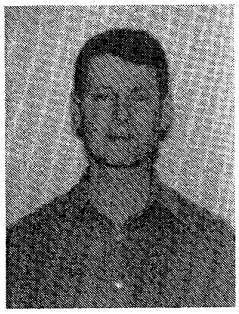

P.R. Lewis
Maritime Operations Division

Paul R. Lewis studied nuclear physics at the University of Melbourne, where he was awarded a PhD in 1990. Since then he has worked in the field of radio physics for the federal government, before joining the Maritime Operations Division of AMRL during 1993. He is currently a research scientist within the Submarine and Ship Sonar group in Sydney.

Contents

1. Introduction

In this brief report we consider the effect of applying a realistic sound speed profile to the determination of Lloyd's Mirror interference fringes, and the subsequent localisation of a source position.

Given a broadband acoustic source located at some range and depth from a sensor, it is possible to determine the (relative) location of this source point from the interference between a direct and a singly reflected beam (Lloyd's Mirror effect) as observed in the received signal frequency spectrum; the frequency spacing of interference minima or maxima being dependent on the source/receiver geometry. Thus, the Lloyd's Mirror (LM) interference will modulate the frequency spectrum. Moreover, if the source is moving, then the time-frequency spectral plot will show these extrema as lines of constant phase difference. These will overlap any narrowband constant frequency emissions from the source and thus will give a temporal modulation of the received narrowband intensity. Even in the absence of broadband emissions, the Lloyd's Mirror effect can be observed through this temporal modulation of the narrowband intensity. Hence, it can offer an important method of determining the source position directly from the measured frequency spectrum of a single receiver

A common approach to determining this position (relative to the receiver) is to assume that the water column is an isotropic, homogeneous medium with a constant sound speed. In this case a simple analytical expression can be derived for the frequencies corresponding to interference extrema. Whilst in some instances a constant speed will be appropriate, more generally this is not a suitable description of the sound speed profile. Here, the degree to which a variable sound speed profile can affect the received interference pattern is considered.

We are motivated in doing this by the need for accurate estimations of the source position to be able to determine absolute source sound pressure levels of, in particular, narrowband emissions, and in the case of a moving source, temporal modulations to the narrow band intensity arising from the LM interference effects.

This report is divided as follows. First, a description is given of the model underlying the calculations. Then follows an overview of the effect of introducing a non-constant sound speed profile, and a discussion of particular case studies. Finally, conclusions are presented.

2. Model Description

For the sake of simplicity, and with little loss of generality, consider a source at a fixed depth, moving with a constant velocity, and having some point of closest approach (CPA) to a receiver. With a constant sound speed profile, rays propagate in straight

lines, and an analytical solution is available for the positions of the LM interference fringes seen in a time-frequency spectrum. We wish to maintain the advantages of an analytical solution, and thus consider a piecewise linear and continuous profile. The range independence and isotropic nature of the medium remain unaltered. A general analytical solution is not available in this case, however with a constant sound speed gradient rays propagate along circular arcs[1]. Thus, an analytical solution for a ray trajectory is available for each profile segment, and raytracing can be done to determine numerically the interference pattern seen in a time-frequency spectrum.

Consider a single layer of the model profile (figure **1**). A ray emitted horizontally will have a radius of curvature ρ_0 determined by the sound speed gradient γ[1],

$$\rho_0(z_{in}) = -\frac{C_S(z_{in})}{\gamma}$$

where z_{in} is the ray starting depth relative to the layer starting depth (z_0) and $C_S(z_{in}) = C_S^0(z = z_0) + \gamma \cdot z_{in}$ is the speed of sound at this depth. For any other ray emitted at some angle θ_{in} to the horizontal, the radius of curvature ρ is greater, with the centre of curvature lying at a depth ρ_0 below the layer depth (figure **1**). That is

$$\rho = \frac{\rho_0(z_{in})}{\cos\theta_{in}}.$$

Simple geometry then defines the quantities of interest. For a ray starting at a depth z_{in} at angle θ_{in} and terminating at depth z_{out} at angle θ_{iut}, the change in range δR is

$$\delta R = \rho \cdot (\sin\theta_{out} - \sin\theta_{in}),$$

the change in depth is

$$\begin{aligned}\delta D &= \rho \cdot (\cos\theta_{in} - \cos\theta_{out}) \\ &= \rho_0 - \rho \cdot \cos\theta_{out}\end{aligned}$$

and the increment in path length is

$$\delta L = \rho \cdot (\theta_{out} - \theta_{in}).$$

The sign convention in use is that downward rays have positive angles, and $z_{in}, z_{out} \geq z_0 \geq 0$. To determine the interference effects between two curved rays, we need to consider the transit time difference of the two ray paths. The transit time along a path S is

$$\delta T = \int_S \frac{dS}{C_S(S)}.$$

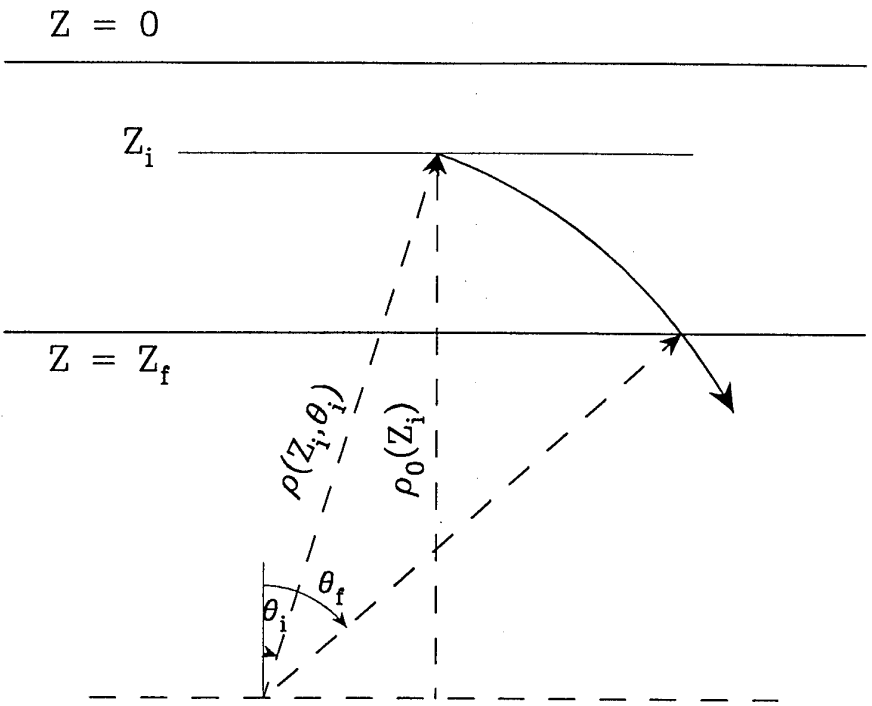

Figure 1: Single layer ray geometry. The ray with radius of curvature ρ *starts at depth* Z_i *below the top of the layer and terminates at depth* Z_f.

Using

$$\begin{aligned} z &= \rho_0 - \rho \cdot \cos\theta \\ C_s(z) &= C_s(z_{\text{in}}) + \gamma \cdot z \\ &= C_s(z_{\text{in}}) + \gamma \cdot \rho_0 - \gamma \cdot \rho \cdot \cos\theta \\ &= -\gamma \cdot \rho \cdot \cos\theta \end{aligned}$$

and

$$dS = \rho \cdot d\theta$$

we obtain

$$\begin{aligned} \delta T &= -\frac{1}{\gamma} \int_{\theta_{\text{in}}}^{\theta_{\text{out}}} \frac{d\theta}{\cos\theta} \\ &= \frac{2}{\gamma} \left\{ \text{atanh}(\tan(\frac{\theta_{\text{in}}}{2})) - \text{atanh}(\tan(\frac{\theta_{\text{out}}}{2})) \right\} \end{aligned}$$

These form the basic equations with which a ray can be traced from a source to a receiver. In the calculations the interest is in the interference effects arising from a direct and a singly reflected ray. Hence, the aim is to determine the transit times of these two rays. For the case of broadband emissions, the transit time difference is used in conjunction with a *desired* phase difference to define a frequency (eg. the frequency at which the interference fringe of a given order occurs), whilst for

emissions, the frequency defines a phase difference, and thus for a moving source a temporal intensity envelope.

For a surface reflected ray a π phase shift is introduced, and the frequencies f_n for order **n** corresponding to interference extrema are given by

$$f_n^{\min} = (n+1)\cdot\left|\frac{1}{\delta T_{\text{direct}} - \delta T_{\text{reflect}}}\right|$$

$$f_n^{\max} = (n+\tfrac{1}{2})\cdot\left|\frac{1}{\delta T_{\text{direct}} - \delta T_{\text{reflect}}}\right| \qquad \text{for } n = 0,1,\ldots$$

For bottom reflection, the extrema frequencies are exchanged. Each order **n** corresponds to a particular fringe in the time-frequency spectrum.

For later identification purposes, CR and SR will refer to the curved and straight line ray propagation models respectively.

3. Lloyd's Mirror Calculations

Two approaches to assessing the interference effects arising from the CR model profile have been taken. Firstly, a set of realistic profiles is considered, with the intention of drawing some more general conclusions concerning the differences between the SR and CR models. Specific profiles, together with data, are then considered, and serve to highlight differences between the two models. To avoid complications that may arise with the bottom layer, only surface reflections are considered. This is a reasonable assumption, since for many situations of interest the water depth is large and bottom bounce interference effects will be diminished *via* signal attenuation and will correspond to very low frequency fringes.

3.1 Overview of CR Model Results

A set of twelve sound speed profiles has been selected, covering six locations about the Australian coast, and two seasons of the year. Each was obtained from the TESS[2)] database, wherein sound speed profiles are gridded at 1° intervals. Each databased profile is selected from a set of profiles measured from within the appropriate grid region, and is assessed as best representing the profile features from this set. Thus, the TESS sound speed profiles can be expected to be realistic whilst giving the general sound speed variations for a particular region. The two seasons are represented by the January and July data. The collection of twelve profiles represents the variation that can be expected in sound speed profiles in the Australian region. A summary of these is given in Table 1 and Figure 3.

Table 1a: Sound speeds and RMS sound speed deviations relative to the surface sound speed as used in the calculations described in section 3.1. Data is for the month of January.

Depth (m)	Tasman Sea		off Brisbane		Coral Sea		Exmouth Gulf		off Perth		Great Aust. Bight	
	C_s (m s^{-1})	$\langle C_s \rangle$ (m s^{-1})	C_s (m s^{-1})	$\langle C_s \rangle$ (m s^{-1})	C_s (m s^{-1})	$\langle C_s \rangle$ (m s^{-1})	C_s (m s^{-1})	$\langle C_s \rangle$ (m s^{-1})	C_s (m s^{-1})	$\langle C_s \rangle$ (m s^{-1})	C_s (m s^{-1})	$\langle C_s \rangle$ (m s^{-1})
0.00	1524.9	0.0	1537.0	0.0	1543.3	0.0	1542.8	0.0	1525.5	0.0	1516.0	0.0
10.0	1524.6	0.2	1536.8	0.1	1543.0	0.2	1542.8	0.0	1525.2	0.2	1515.8	0.1
20.0	1524.0	0.5	1536.4	0.3	1542.9	0.3	1542.9	0.0	1524.9	0.3	1515.8	0.1
30.0	1522.8	1.0	1535.5	0.7	1542.0	0.6	1540.3	0.8	1524.4	0.6	1516.0	0.1
50.0	1519.1	2.7	1531.4	2.4	1540.4	1.4	1537.7	2.5	1523.3	1.2	1517.1	0.4
75.0	1515.4	5.0	1528.1	4.7	1538.4	2.6	1536.6	3.9	1520.4	2.4	1512.7	1.0
100.0	1513.1	6.9	1525.3	6.6	1535.1	4.0	1533.9	5.1	1517.7	3.8	1510.4	2.4
125.0	1511.4	8.3	1523.0	8.2	1532.9	5.5	1529.6	6.7	1515.7	5.2	1510.1	3.4
150.0	1510.5	9.5	1521.2	9.7	1530.3	6.9	1525.7	8.7	1513.7	6.5	1508.6	4.1
200.0	1508.0	11.4	1519.9	11.7	1523.5	10.2	1519.7	12.6	1509.5	9.0	1506.7	5.5

Table 1b: Sound speeds and RMS sound speed deviations relative to the surface sound speed as used in the calculations described in section 3.1. Data is for the month of July.

Depth (m)	Tasman Sea		off Brisbane		Coral Sea		Exmouth Gulf		off Perth		Great Aust. Bight	
	C_s (m s^{-1})	$\langle C_s \rangle$ (m s^{-1})	C_s (m s^{-1})	$\langle C_s \rangle$ (m s^{-1})	C_s (m s^{-1})	$\langle C_s \rangle$ (m s^{-1})	C_s (m s^{-1})	$\langle C_s \rangle$ (m s^{-1})	C_S (m s^{-1})	$\langle C_s \rangle$ (m s^{-1})	C_s (m s^{-1})	$\langle C_s \rangle$ (m s^{-1})
0.00	1511.8	0.0	1524.8	0.0	1535.8	0.0	1534.7	0.0	1519.6	0.0	1509.7	0.0
10.0	1511.8	0.0	1524.9	0.1	1535.7	0.1	2534.7	0.0	1519.7	0.1	1509.5	0.1
20.0	1511.9	0.0	1524.9	0.1	1535.6	0.1	1534.8	0.0	1519.8	0.1	1509.6	0.1
30.0	1511.9	0.1	1525.0	0.1	1535.7	0.1	1534.8	0.1	1519.7	0.1	1509.6	0.1
50.0	1511.9	0.1	1525.0	0.2	1536.3	1.2	15334.8	0.1	1519.4	0.1	1510.3	0.2
75.0	1511.7	0.1	1526.6	0.6	1536.2	0.3	1535.8	0.4	1518.7	0.4	1510.1	0.3
100.0	1511.4	0.1	1526.4	1.0	1531.8	1.1	1533.2	0.5	1517.9	0.7	1509.6	0.3
125.0	1510.7	0.4	1524.2	1.0	1531.1	2.2	1530.2	1.5	1516.7	1.2	1508.6	0.4
150.0	1511.7	0.4	1524.1	0.9	1527.8	3.3	1526.6	2.9	1515.2	1.9	1506.5	1.0
200.0	1509.5	0.8	1522.7	1.1	1521.7	6.3	1519.8	6.4	1510.7	3.8	1506.5	1.8

In each case the CR model is compared to the SR model based on the *surface* sound speed. The comparison is between the predicted frequencies corresponding to an interference minimum for a series of source ranges and depths, at several set receiver depths. Figure 2 shows a typical LM fringe pattern for orders **n**=0, 1. The solid line shows the fringes predicted using the CR model, with the dashed line corresponding to the SR model fringes. A single layer linear sound speed profile (gradient γ = -0.1 ms^{-1}/m and C_s = 1500 ms^{-1}) was used. Clearly the CR model results in a fringe system of greater curvature than the SR model, for which the fringes are asymptotically linear, and at some range (or time) the CR **n**=0 fringe will overlap the SR **n**=1 fringe. This motivates the use of the fractional difference

$$\eta = \frac{f_0^{CR} - f_0^{SR}}{f_1^{SR} - f_0^{SR}}$$

as a measure of the similarity of the two model predictions, where the model frequencies are in each case determined using the same parameter set. For the curvature of the rays to have little effect on the LM pattern, $\eta \approx 0$. With $\eta = 0.5$, the CR model minimum of order **n** matches the SR model maximum of order (**n**+1), indicating a significant deviation of the CR model predictions from the SR model predictions. Hence, as a measure of the dissimilarity of the two model predictions, a value $\eta > 0.25$ is assumed. It is noted that η describes the differences in the *shapes* of the frequency/time curves arising from the two models.

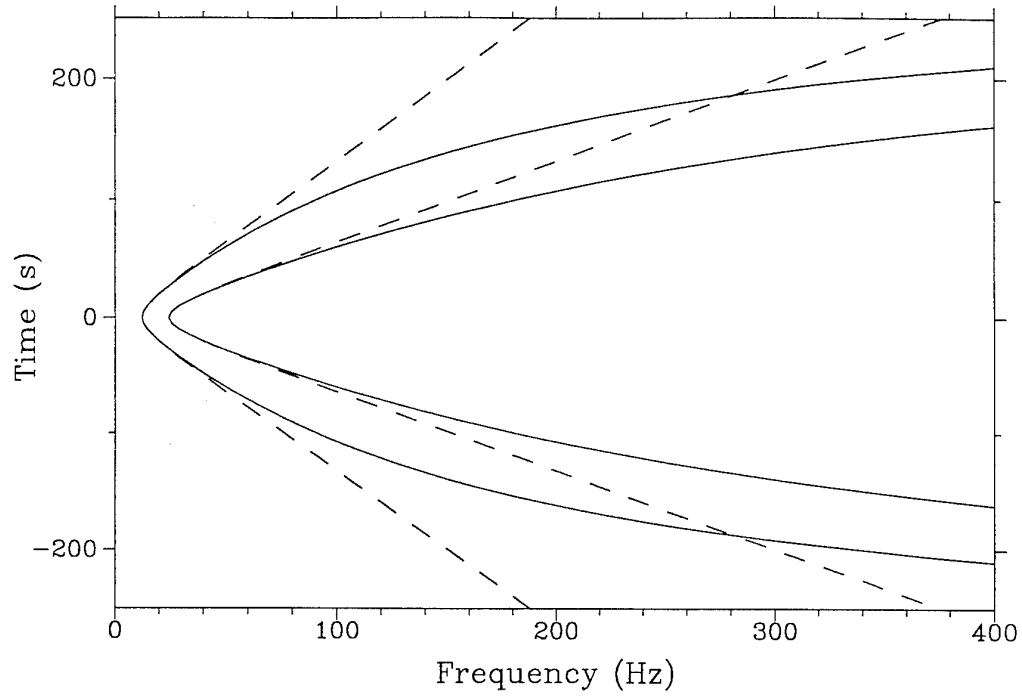

Figure 2: Surface reflections Lloyd's mirror destrucive interference fringes for orders n=0 and 1. The solid line represents the results of a single layer with a sound speed gradient of -0.1 ms⁻¹/m; the dashed line, a single layer with a constant sound speed profile. In each case the surface sound speed is 1500 ms⁻¹. The system geometry is: CPA range = 100 m, speed = 10 ms⁻¹, source depth = 100 m and receiver depth = 100 m.

The deviation η as a function of source depth and source range for several receiver depths is shown in the contour plots, figure **4**. In each case, the heavy solid line shows the η=0.25 contour. Figure **3** shows the corresponding sound speed profiles. Only ranges to 2000 m and the upper 200 m surface layer are considered. Over this depth, the profiles exhibit RMS sound speed deviations $<C_S>$, with respect to the surface sound speed, of ~5–10 ms^{-1} in January and ~1–6 ms^{-1} in July, and maximum gradients of ~0.1–0.2 ms^{-1}/m. Several profiles (notably in July) show only small variations of sound speed with depth.

It is clear from figure **4** that there is a steady increase in the effect of ray curvature as the range is increased, as might be expected. Changes in the source and receiver depths result in a less pronounced effect, and in several cases ray curvature is of lesser importance with increasing depth. First consider the profiles with the (largest) steadily increasing gradients (Exmouth Gulf, off Perth, Tasman Sea, off Brisbane & Coral Sea January profiles). All have a similar form, and show similar curvature effects as indicated by η. Typically, critical ranges (defined as the range at which η=0.25) of 600–1500 m are found, with this range increasing as the maximum gradient decreases. We also note that there is a generally smooth evolution in the value of η arising from changes in the source and receiver depths. For profiles such as those for the Exmouth Gulf and the Great Australian Bight in January, an approximate iso-speed layer exists, and expectably only when the depths below this layer are sampled do we see a steady increase in η with range. A separate feature arising from the geometries of the direct and reflected rays is seen at shallow source and receiver depths. In this case values of η much larger than is typical for the particular profile can be obtained (for example, the Coral Sea January and the Great Aust. Bight profiles). This arises from the direct and reflected rays having increasingly similar optical path lengths, or decreasing time differences. This will occur for even small gradient profiles, although the matching range will increase as the magnitude of the gradient decreases. At larger depths, this feature will be observable at larger ranges.

The profiles can be grouped according to whether or not the sound speed has a maximum at some depth other than at the surface. Of those that do (all July & Exmouth Gulf and Great Aust. Bight January profiles), the presence of local maxima leads to shadow zone effects as well as possibly the features already noted. This shadow zoning is possible even in the presence of small gradients, (see figure **4b** where generally $\eta \approx 0$). The degree to which it will be important depends on the specific depth and range geometry. In practice such zones will not affect the time-frequency spectrum insofar as they will result in a restricted range of observation, but otherwise will not greatly affect the shape of the fringe pattern.

In as much as these profiles represent a typical variation, evidently ray curvature can play an important role at close range. In several cases, depending on the details of the sound speed profile and the source/receiver geometry, the effects are pronounced at ranges of about 600 – 700m.

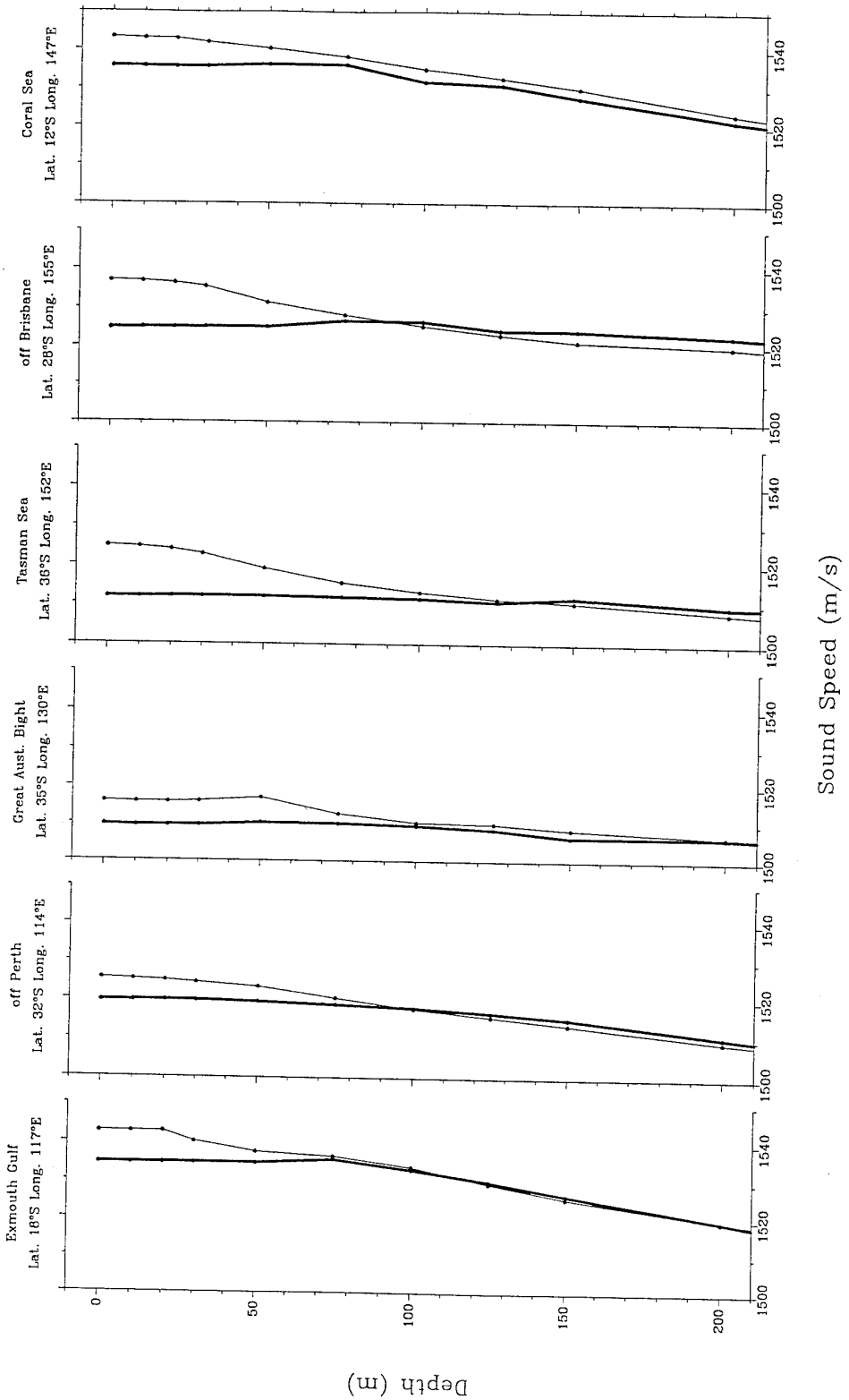

Figure 3: Sound speed profiles extracted from the TESS database. The locations are as indicated above each figure. The light line shows the summer (January) profile, with the heavy line showing the winter (July) profile. Only the surface 200 m are shown.

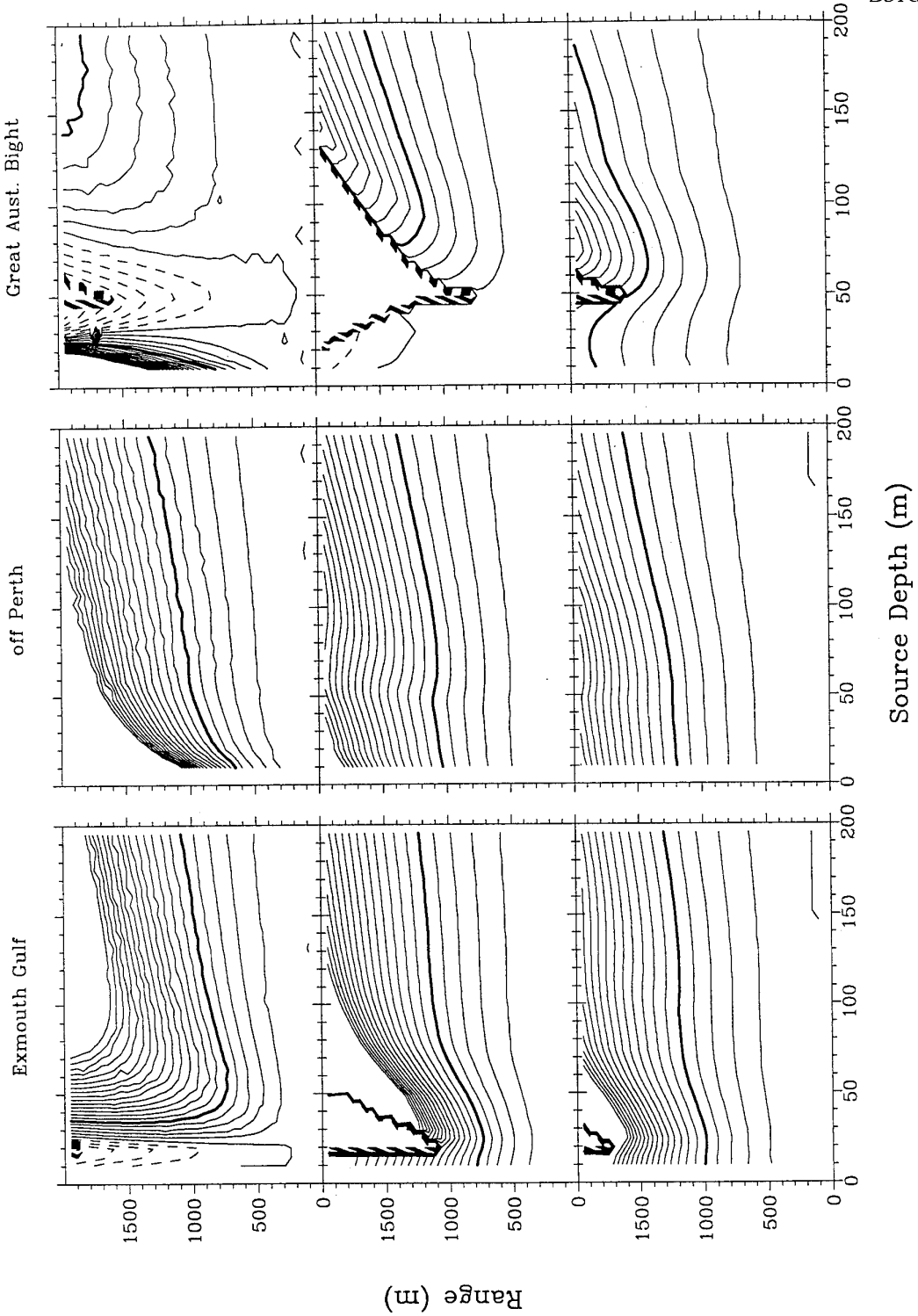

Figure 4a: Contour plots of the fraction deviation η, as defined in the text, for each location during the summer. The contour spacing is 0.05, and the 0.25 contour is indicated by the heavy line. The dashed lines show negative values of η. The upper row is for a receiver depth of 10 m, the middle for 80 m and the lower row is for a depth of 160 m. In each case η increases with range.

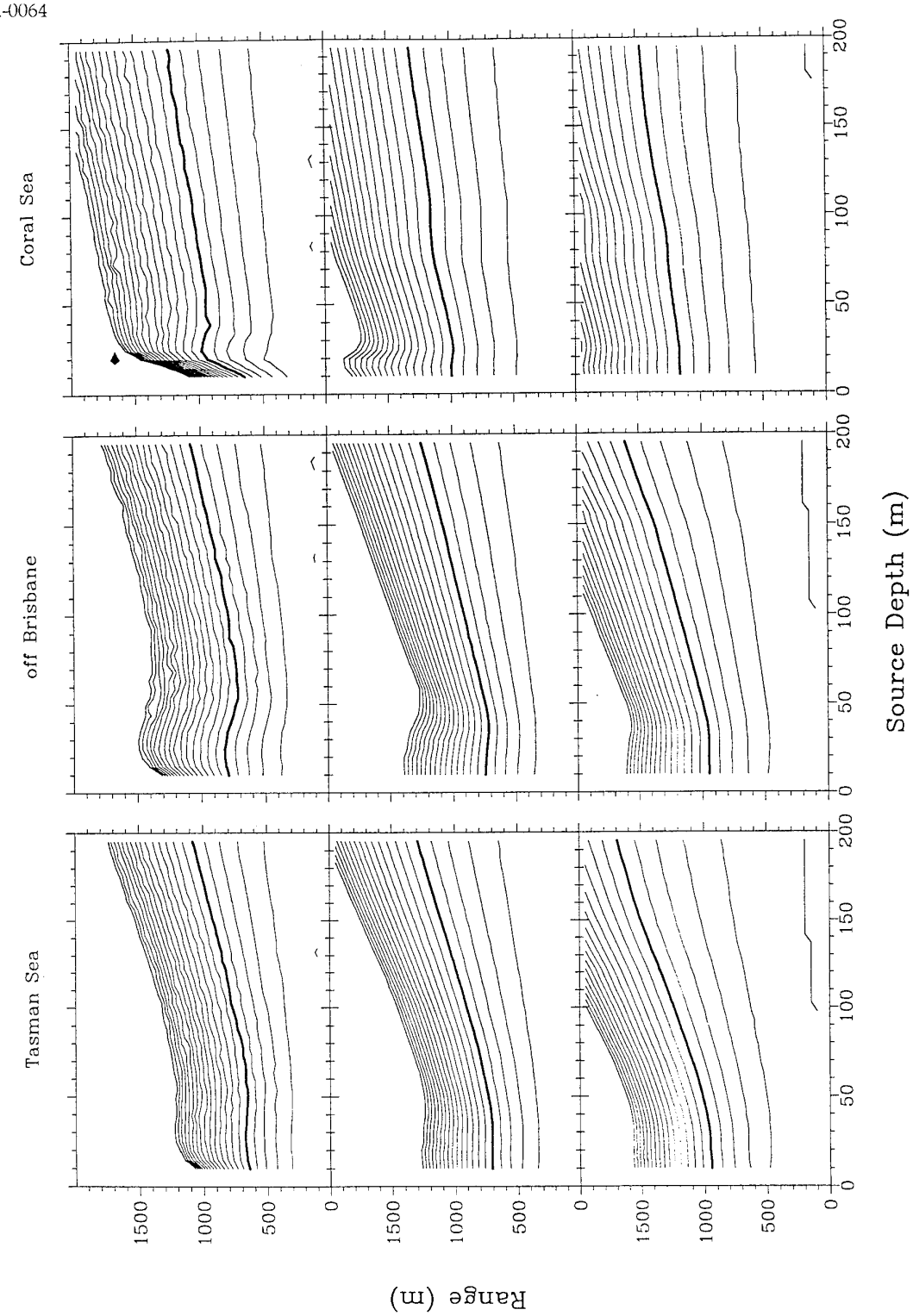

Figure 4a (Contd): Contour plots of the fraction deviation η, as defined in the text, for each location during the summer. The contour spacing is 0.05, and the 0.25 contour is indicated by the heavy line. The dashed lines show negative values of η. The upper row is for a receiver depth of 10 m, the middle for 80 m and the lower row is for a depth of 160 m. In each case η increases with range.

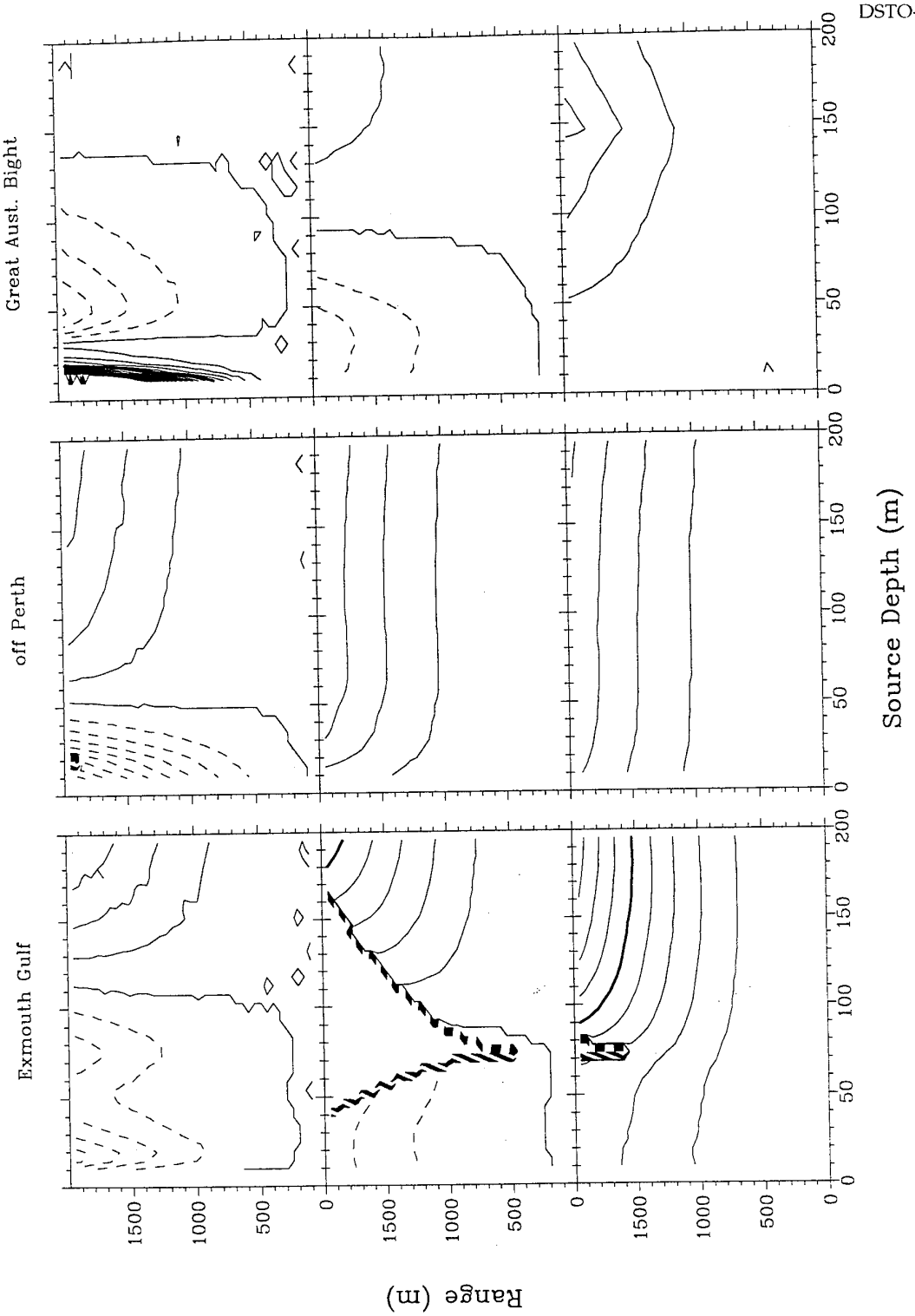

Figure 4b: Contour plots of the fraction deviation η, as defined in the text, for each location during the winter. The contour spacing is 0.05, and the 0.25 contour is indicated by the heavy line. The dashed lines show negative values of η. The upper row is for a receiver depth of 10 m, the middle for 80 m and the lower row is for a depth of 160 m. In each case η increases with range.

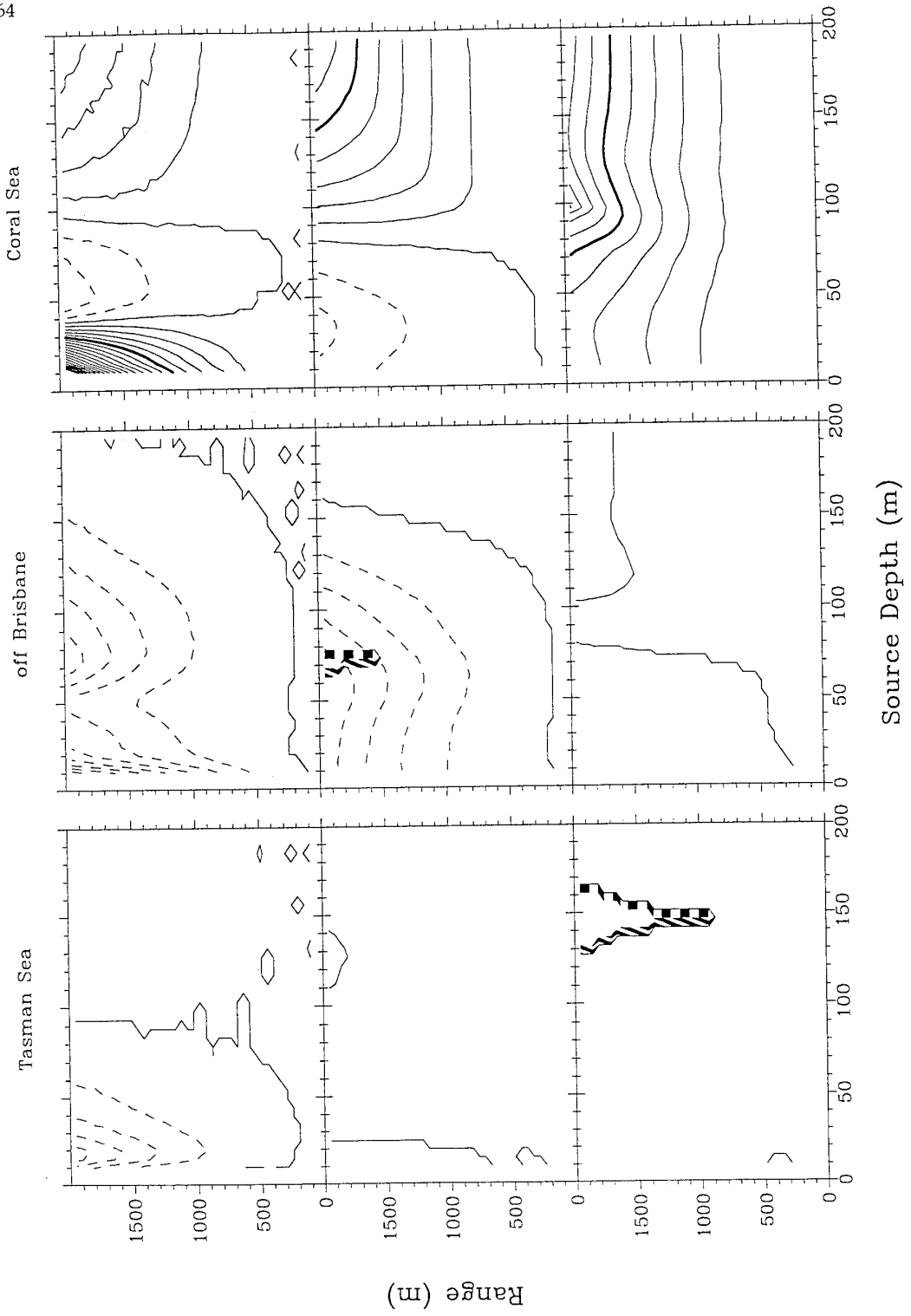

Figure 4b (Contd): Contour plots of the fraction deviation η, as defined in the text, for each location during the winter. The contour spacing is 0.05, and the 0.25 contour is indicated by the heavy line. The dashed lines show negative values of η. The upper row is for a receiver depth of 10 m, the middle for 80 m and the lower row is for a depth of 160 m. In each case η increases with range.

One measure of the effect a particular profile will have on the η(Range, Depth) distribution is the "average" sound speed gradient over a given depth as defined by

$$G(D) \equiv < C_s(D) > / D$$

where $<C_s(D)>$ is the RMS sound speed deviation at depth D. This is motivated by the reflected ray needing to sample the entire sound speed profile between the source and the surface, and the larger the variation in the sound speed over this path, the larger the effects of ray curvature on the path length (or transit time). From inspection of the various contour plots, figure **4**, and the values **G** deduced from table **1**, it appears that a *rough* rule for the adequacy of the SR model is $\mathbf{G} < 0.01$ ms^{-1}/m over the depths of interest (this corresponds to a nearly constant temperature profile). This value is also suggested in calculations done using a single layer of constant gradient. This is for a range to 2000 m, and the value will decrease as the range is increased. As the details of any LM pattern will depend on the specific sound speed profile and the source/receiver geometry, such figures of merit are of limited value, and a direct calculation of η (or the LM fringe pattern itself) would be a more productive assessment of the adequacy of the SR model in any particular case.

3.2 Data Comparisons

Three sets of time-frequency data, previously reported in the AJAAC bulletin[3-5], are considered. In each case a well-developed Lloyd's mirror pattern is evident and, owing to the large water depths at each location, can be ascribed to surface reflection. Further, source speeds are known from independent analysis of the observed narrowband frequency doppler shifts. It is assumed, and the data support this, that over the acquisition period each source was travelling at constant depth and velocity.

There are five variables of interest: the receiver depth, the source depth and CPA range, the time of closest approach and the source speed, with the latter three defining the source range as a function of time. It can be assumed that the receiver depth is known, and the aim is to replicate the observed LM broadband fringe pattern and thus deduce the source variables. As with the SR model, the CR model doesn't in general uniquely specify these variables and to resolve the ambiguity one of the source CPA range, depth or source speed must be known. In these examples the source speed is specified, being known from earlier analysis. The remaining source parameters have been determined using the SR and CR models via a weighted LS optimisation on a selected number of LM fringes. A weighting designed to favour the data nearest to the CPA time is chosen. This will only be of significance in those cases where the assumed model is inappropriate. We consider each case separately.

3.2.1 Case A

These data[3] clearly show the inadequacies of the SR model. Based on the CR model analysis, ranges from ~1200–3400m, and corresponding to fractional deviations of $0.08 < \eta < 1.0$, are sampled by the data. As no experimental sound speed profile was available, the appropriate profile was obtained from the TESS[2] database, and is shown in figure **5a**. Based on the receiver type, the receiver depth was assumed to be 305m. Table **2** summarises the "best fit" parameters for each model. The corresponding LM fringe patterns are shown in figure **6**.

Clearly, the data show fringes with significant curvature, and that whilst the SR model is incapable of reproducing this, the CR model well matches the observed fringe shape. Furthermore, the resulting "best fit" parameters are markedly different for the two models. The use of the SR model in this circumstance would have important consequences for the analysis of any narrowband lines in the time-frequency spectrum. If the underlying intrinsic intensity profile of such a line were desired, then LM interference corrections and $1/R^2$ losses based on the SR model would be inappropriate and lead to substantial errors. If in addition several such lines were considered together, inconsistent results for the source location would result because of the incorrect placement of interference minima at the different frequencies.

3.2.2 Case B

These data[4] represent another example of the inappropriateness of the SR model. Ranges based on the CR model "best fit" parameters cover ~1000–2400m, with $0.1 < \eta < 1.4$. Again, the receiver depth is assumed to be 305m. In this example, a sound speed profile recorded from a nearby location and time was available[4]. This is shown in figure **5b**, whilst the "best fit" parameters are included in table **2**. The LS fit results are shown in figure **7**. It is again evident that the SR model cannot reproduce the data, with the calculated fringes showing too little curvature. The CR model gives an excellent representation of the data. As before, the "best fit" parameters for each model are significantly different, and the comments above concerning narrowband lines are relevant.

Table 2: Weighted least squares fit parameters for cases A, B & C. Parameter sets for the curved (CR) and straight line (SR) ray models are shown. In each case the receiver depth and source speed were fixed at the indicated values. The resulting curves are shown in figures 6-10.

parameter	Case A		Case B			Case C	
	CR[1)]	SR	CR[2)]	CR[1)]	SR	CR[1)]	SR
CPA time[a)] (s)	372.5	372.3	407.9	406.3	405.3	357.3	357.4
CPA range[b)] (m)	1244.3	945.2	958.2	733.3	566.8	823.0	712.4
Source depth (m)	198.0	144.2	162.2	120.4	96.4	74.7	62.7
Source speed[c)] (m s^{-1})	11.4	11.4	8.1	8.1	8.1	8.7	8.7
Receiver depth[d)] (m)	305.0	305.0	305.0	305.0	305.0	305.0	305.0

a) time offset is arbitrarily chosen
b) horizontal range
c) set at value determined from separate doppler shift analysis of narrow band lines
d) depth unknown, but based on receiver type
1) fit based on TESS sound speed profile
2) fit based on measured sound speed profile

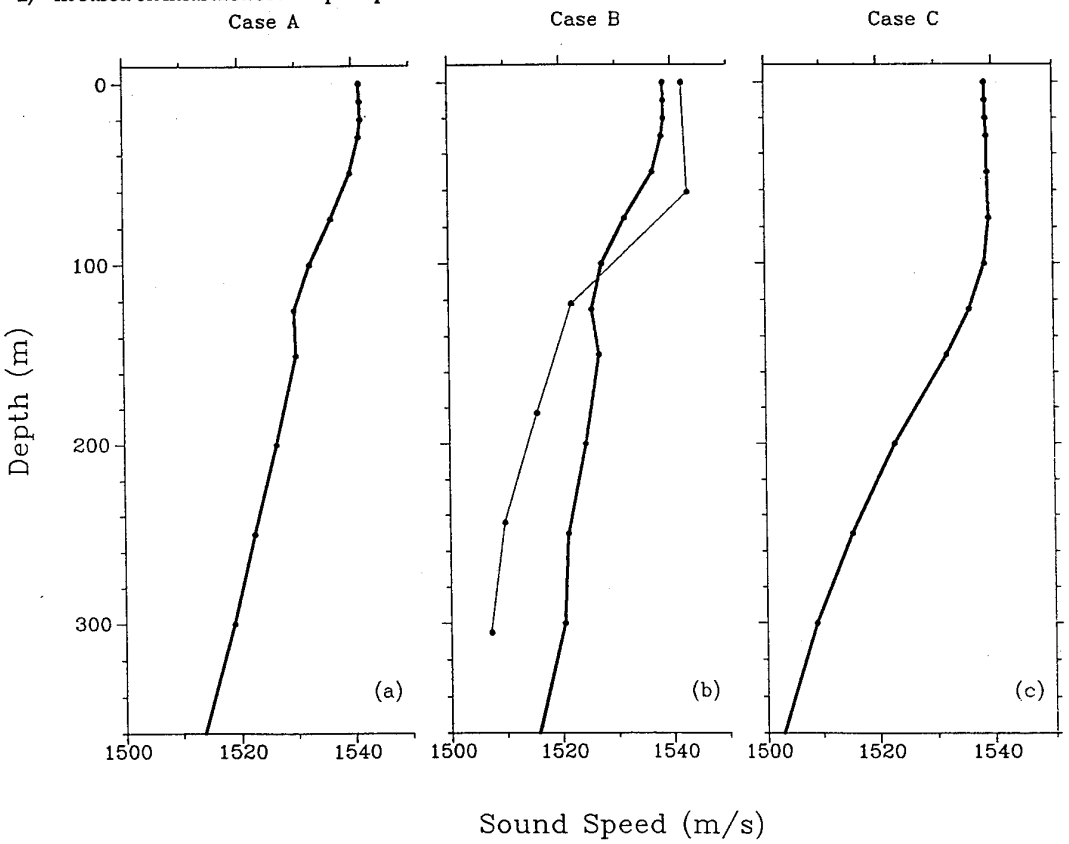

Figure 5: Sound speed profiles used in the CR model calculations of section 3.2. The heavy line shows the profiles extracted from the TESS data base and the light line in (b) shows a profile measured close to the location of the case B data acquisition. Only the surface 350 m are shown.

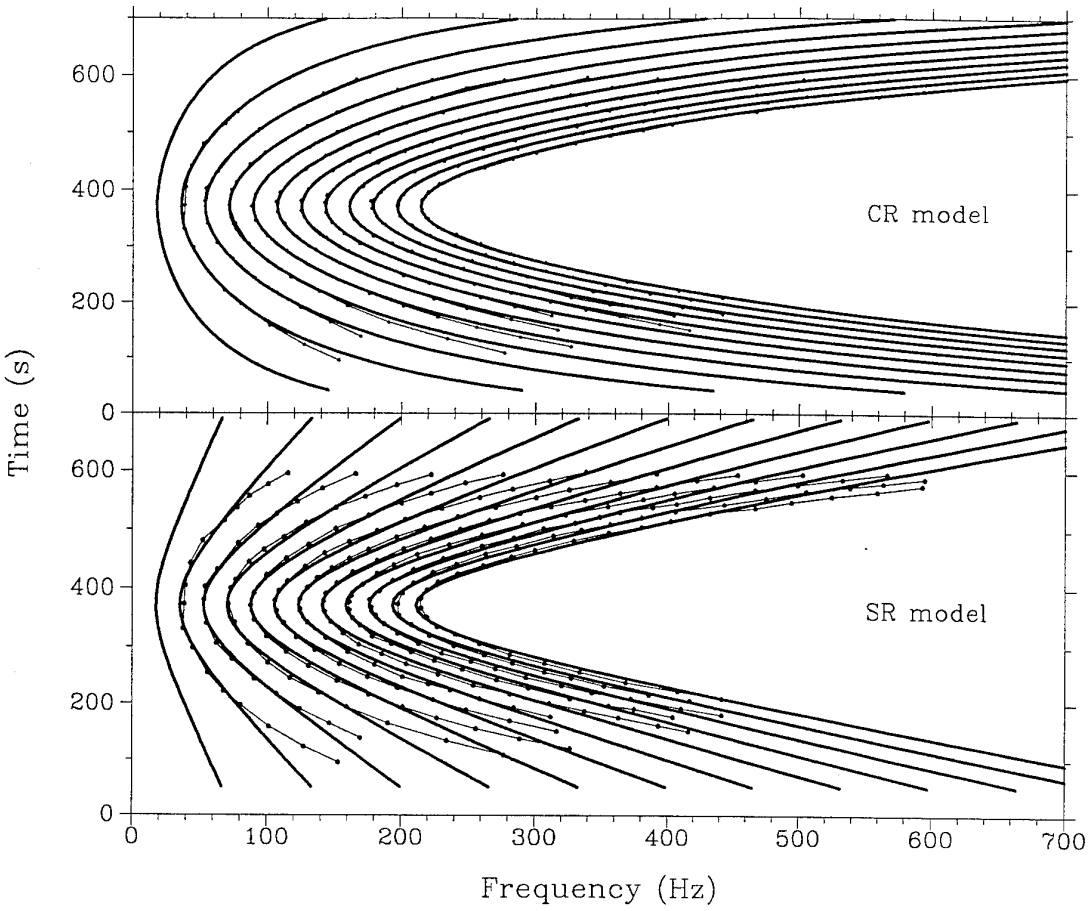

Figure 6: Surface reflection Lloyd's mirror interference minima contours for orders n=1-11. The data are described for case A, section 3.2.1. The heavy lines show the LS optimal fit to the data, based on the TESS profile of fig. 5a (upper figure) or a constant sound speed profile (lower figure). The resulting LS parameters are given in table 2.

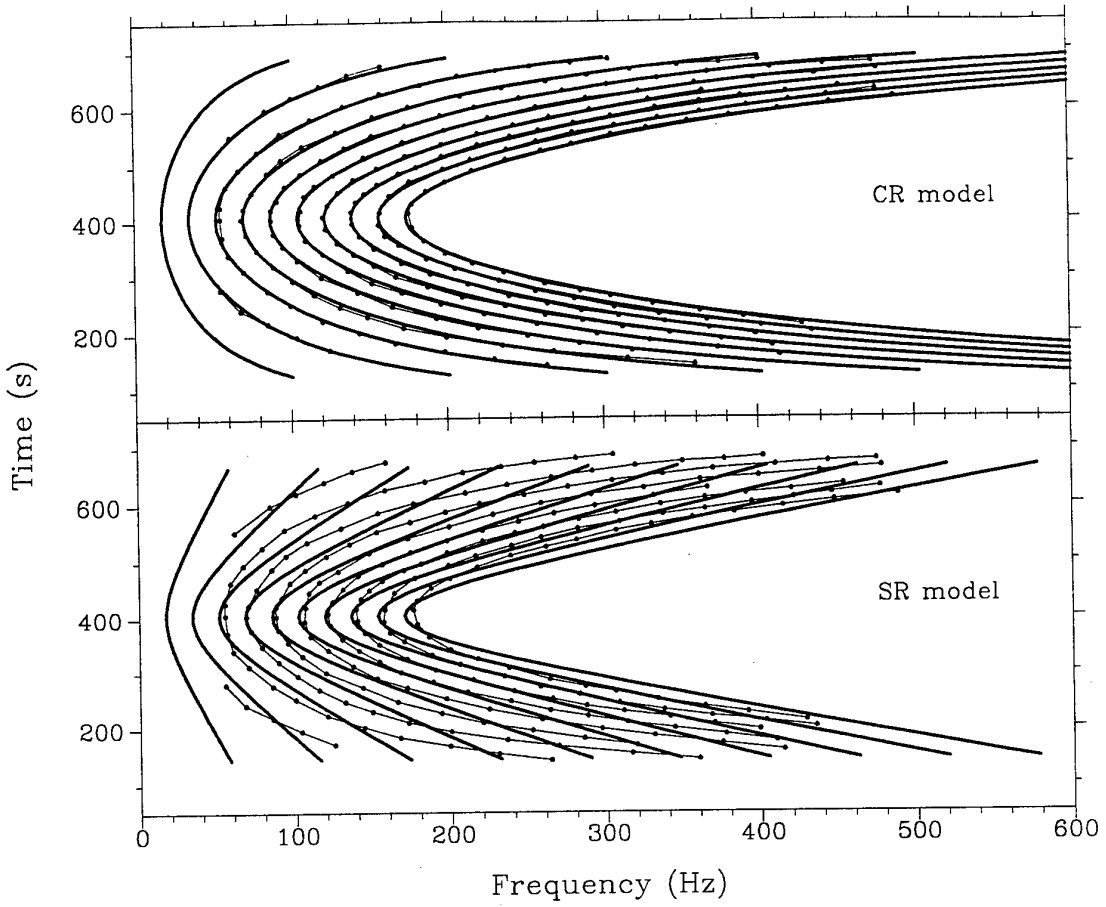

Figure 7: Surface reflection Lloyd's mirror interference minima contours for orders n=1-10. The data are described for case B, section 3.2.2. The heavy lines show the LS optimal fit to the data, based on the measured profile of fig. 5b (upper figure), as described in the text, or a constant sound speed profile (lower figure). The resulting LS parameters are given in table 2.

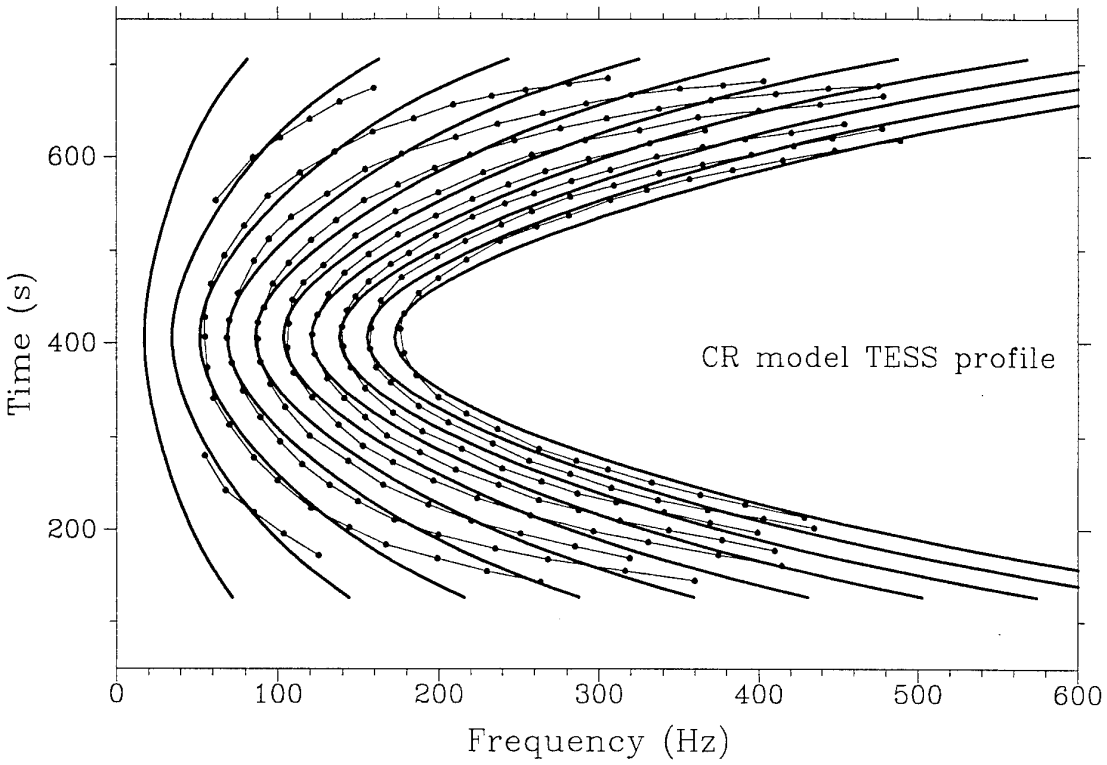

Figure 8: Surface reflection Lloyd's mirror interference minima contours for orders n=1-10. The data are described for case B, section 3.2.2. The heavy lines show the LS optimal fit to the data, based on the alternative, TESS, profile of fig. 5b. The resulting LS parameters are given in table 2.

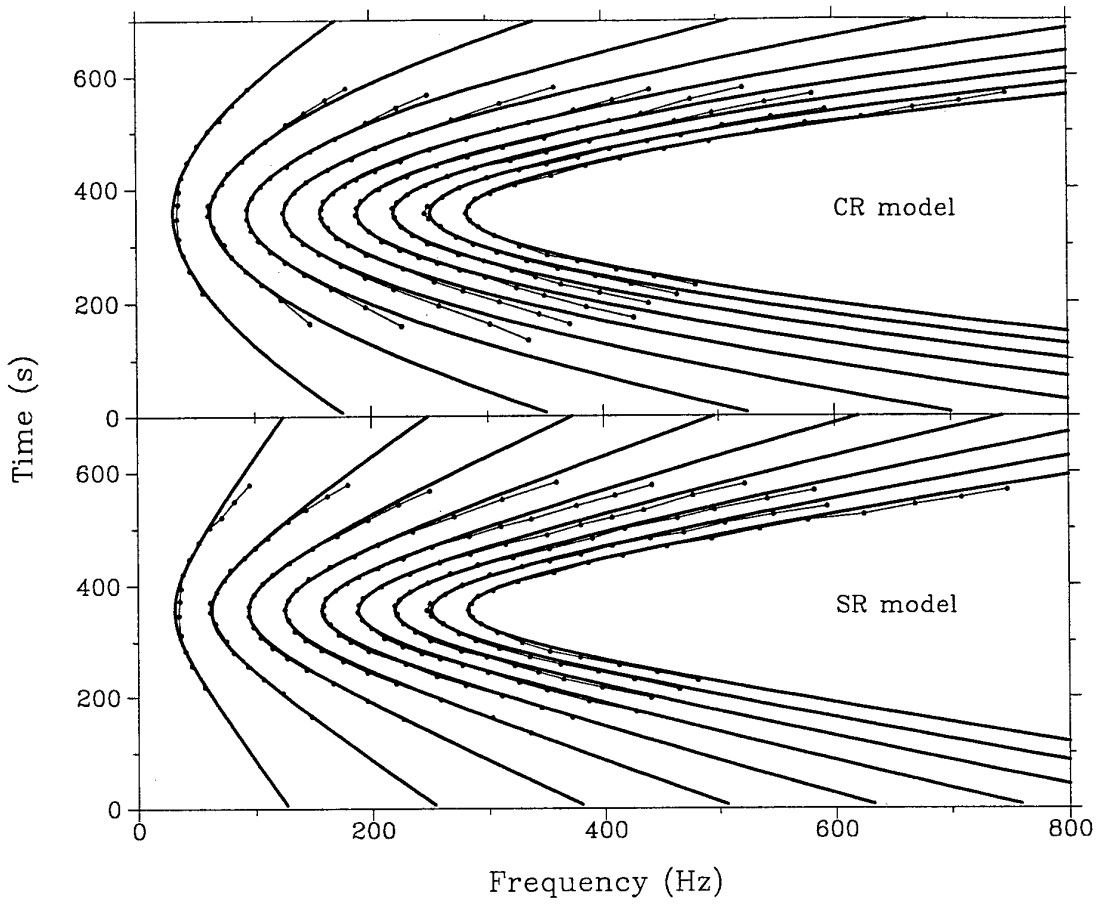

Figure 9: Surface reflection Lloyd's minor interference minima contours for orders n=0-8. The data are as described for case C, section 3.2.3. The heavy lines show the LS optimal fit to the data, based on the TESS profile of fig. 5c (upper figure) or a constant sound speed profile (lower figure). The resulting LS parameters are given in table 2.

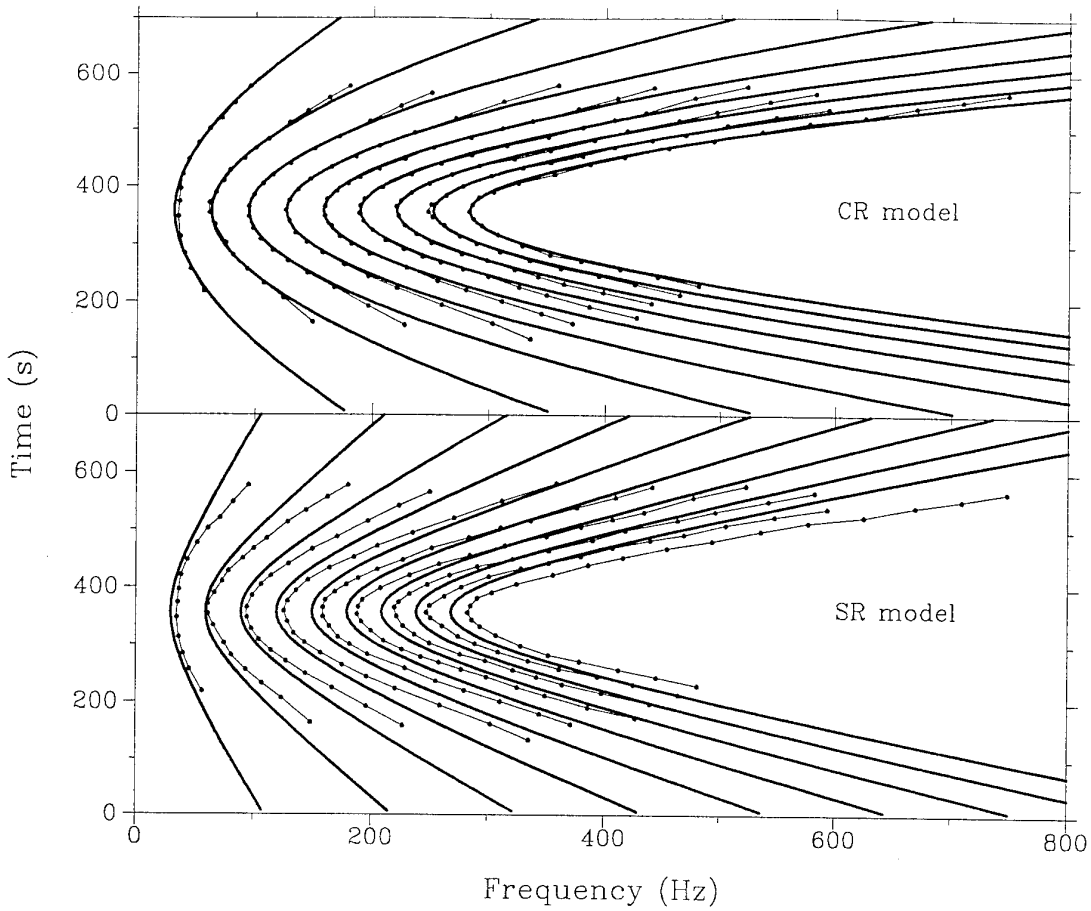

Figure 10: Surface reflection Lloyd's mirror interference minima contours for orders n=0-8. The data are as described for case C, section 3.2.3. The heavy lines show the model calculations based on the TESS profile of fig. 5c (upper figure) or a constant sound speed profile (lower figure). The CR source trajectory parameters given in table 2 are used in each case.

It is also possible to test the effect of using a different sound speed profile; in this case the profile obtained from the TESS[2] database. Given that sufficient sensitivity exists for a discernible difference between the SR and CR model results, it not unreasonable to expect that the results will, to a lesser degree, be sensitive to the specific sound speed profile. This profile is also shown in figure **5b** by the heavy solid line, where it can be seen that only qualitative agreement to the "true" profile is obtained. Lloyd's mirror calculations based on this latter profile are shown in figure **8**. Now only qualitative agreement with the data can be obtained using this sound speed profile, and the resulting "best fit" parameters (included in table **2**) do not agree with the earlier values based on the measured profile. Differences in the source depth and the CPA range of ≈25% are noted. The quality of this fit, lies between that for the SR model and the CR model based on the measured profile.

3.2.3 Case C

This last example[5] is interesting because the LM fringe pattern is not present for the larger source ranges. Based on the CR model calculations, ranges of ~800–1900m are sampled, and we find $0.06<\eta<0.3$. As for case **A**, the sound speed profile is obtained from the TESS[2] database, and is shown in figure **5c**. The resulting LM fringe patterns based on the two models are shown in figure **9**, with the "best fit" parameters included in table **2**.

As suggested by the smaller values of η, the SR and CR models are equally capable of reproducing the observed fringe system shown in figure **9**. We note, however, that the "best fit" parameters derived using the two models differ by ~15%. Indeed, as the value of η is not dependent on the interference fringe order, a small value can still lead to a large discrepancy between the matches of the two models to the data *at higher orders* since any difference is amplified by the order number. This is shown in figure **10** where the CR and SR model curves are calculated using the same parameter set (the Case C CR model parameters of table **2**). At the CPA time, $\eta\approx0.06$ but for the $n=8$ fringe, a large mismatch between the two models is found. Thus, although the value of η can give an indication of whether the SR model will be able to match the data, it will not necessarily indicate the suitability of the deduced source location.

4. Conclusions

The consequences of including realistic sound speed profiles on the Lloyd's mirror interference pattern have been considered, and the need to use such profiles has been demonstrated. Using ray tracing it is found that ray curvature arising from a piecewise linear sound speed profile can cause significant changes in the frequencies of the LM interference extrema for a given source/receiver geometry, and that such effects can occur within the ranges of interest for passive sonar detection. It is also the

being considered, together with the source and receiver depths. Except where the sound speed gradient is small (<0.01 ms^{-1}/m for ranges <2000m) ray curvature is potentially important. Ranges of 600 - 700m have been found to be sufficient to cause marked deviations from the constant sound speed model. By considering a fractional deviation function, it is possible to visualise the source range-depth regions that potentially will be significantly affected by ray curvature.

Three particular sets of data for sources with fixed velocities and depths were considered . Each was chosen because clear broadband fringe systems are present for times that correspond to large source/receiver ranges, and thus more readily elucidate any effects of ray curvature. It is more usual that such a broadband pattern is not present, however as mentioned in the introduction, the effects of Lloyd's mirror interference can and often will be present in the (stronger) narrowband signals. These data demonstrate the inadequacies of the straight line propagation approach, whereas each set can be explained with the ray curvature model. It is also found that the inferred source location is very dependent on the choice of model. Thus, it is important to ensure the suitability of the applied model, for example, before the theoretical LM pattern is used in estimating either broadband or narrowband sound pressure levels. A poor choice will result in a poor estimation of the intrinsic levels. One example is noted where although a good fit to the interference fringes was obtained with the straight line model, the resulting source location differs between the two models considered. The implication is that care needs to be exercised in ascertaining the applicability of a constant sound speed profile.

For a further example, it was possible to compare the results of calculations using two different sound speed profiles with the same acoustic data. The results indicate that the quality of any fit and the thus derived source parameters will be sensitive to the choice of profile. It is therefore important that a well described true profile (*ie.* one measured temporally and spatially close to the true location) be used. Given the number of potential unknowns, this also suggests that the receiver depth be correctly known, as the specific source/receiver geometry is important in determining the effect of ray curvature for a given sound speed profile. Information that can be obtained from an independent analysis of narrowband lines (*viz.* source speed, approximate CPA range) is also of use, given that a unique solution is not guaranteed from the Lloyd's mirror analysis alone. With this, it should be possible to correctly utilise the information inherently present in the time-frequency spectrum.

5. References

1. Urick R J, *Principles of Underwater Sound* (3rd Edition) McGraw-Hill 1983, pp124-125
2. TESS sonar range prediction program, version 1 (unpublished)
3. AJAAC Bulletin Vol 3 1992, p IV-7
4. AJAAC Bulletin Vol 2 1992, p IV-26
5. AJAAC Bulletin Vol 2 1992, p IV-8

The Effect of Ray Curvature on Lloyd's Mirror Fringe Estimates and Source Localisation

P.R. Lewis

(DSTO-TR-0064)

DISTRIBUTION LIST

Director, AMRL
Chief, Maritime Operations Division
Research Leader, Submarine and Ship Sonar
Research Leader, Sonar Technology and Processing
P.R. Lewis, MOD Sydney
Library, AMRL Maribyrnong
Library, AMRL Fishermens Bend

Chief Defence Scientist (for CDS, FASSP, ASSCM) 1 copy
Director, ESRL
Head, Information Centre, Defence Intelligence Organisation
OIC Technical Reports Centre, Defence Central Library
Officer in Charge, Document Exchange Centre 8 copies
Senior Defence Scientific Adviser
Air Force Scientific Adviser, Russell Offices
Scientific Adviser - Policy and Command
Senior Librarian, Main Library DSTOS
Librarian - AMRL Sydney 2 copies
Librarian, DSD, Kingston ACT
Librarian, Australian Defence Force Academy
Serials Section (M List), Deakin University Library, Deakin University, Geelong 3217
NAPOC QWG Engineer NBCD c/- DENGRS-A, HQ Engineer Centre, Liverpool Military Area, NSW 2174
ABCA, Russell Offices, Canberra ACT 2600 4 copies
Head of Staff, British Defence Research and Supply Staff (Australia)
NASA Senior Scientific Representative in Australia
INSPEC: Acquisitions Section Institution of Electrical Engineers
Head Librarian, Australian Nuclear Science and Technology Organisation
Senior Librarian, Hargrave Library, Monash University
Library - Exchange Desk, National Institute of Standards and Technology, US
Acquisition Unit (DSC-EO/GO), British Library, Boston Spa, Wetherby Yorkshire LS23 7BQ, England
Library, Chemical Abstracts Reference Service
Engineering Societies Library, US
Documents Librarian, The Center for Research Libraries, US
Library, Deakin University
Army Scientific Adviser, Russell Offices - data sheet only
Navy Scientific Adviser - data sheet only
Director General Force Development (Land) - data sheet only
DASD, APW2-1-OA2, Anzac Park West, Canberra ACT - data sheet only
SO (Science), HQ 1 Division, Milpo, Enoggera, Qld 4057 - data sheet only
Counsellor, Defence Science, Embassy of Australia - data sheet only
Counsellor, Defence Science, Australian High Commission - data sheet only
Scientific Adviser to DSTC Malaysia, c/- Defence Adviser - data sheet only
Scientific Adviser to MRDC Thailand, c/- Defence Attache - data sheet only

Commanding Officer, AJAAC, HMAS ALBATROSS, Nowra NSW 2450
C. Lightowler, MOD Salisbury
C. Martin, MOD Salisbury
A.D. Jones, MOD Salisbury
C.L. Davis, MOD Sydney
D.A. McMahon, MOD Salisbury

REPORT NO.	AR NO.	REPORT SECURITY CLASSIFICATION
DSTO-TR-0064	AR-008-927	Unclassified

TITLE

The effect of ray curvature on Lloyd's mirror fringe estimates and source localisation

AUTHOR(S)
P.R. Lewis

CORPORATE AUTHOR
DSTO Aeronautical and Maritime Research Laboratory
GPO Box 4331
Melbourne Victoria 3001

REPORT DATE	TASK NO.	SPONSOR
September 1994	92/259	CO AJAAC

FILE NO.	REFERENCES	PAGES
510/207/0140	5	28

CLASSIFICATION/LIMITATION REVIEW DATE

CLASSIFICATION/RELEASE AUTHORITY
Chief, Maritime Operations Division

SECONDARY DISTRIBUTION

Approved for public release

ANNOUNCEMENT

Announcement of this report is unlimited

KEYWORDS

Acoustic velocity
Sound waves
Sonar detection
Sonar sound analysers
Fringe pattern analysis
Reaction time
Velocity measurement analysis

ABSTRACT

A knowledge of the interference between direct, surface and bottom refelected rays emanating from a moving underwater source can be used to determine the source-detector relative positions. Using simple ray tracing, the frequency-time interference patterns for a broadband frequency source arising when the propagating medium has a piecewise linear sound speed profile are considered, and are compared with those for a constant sound speed. It is found that even small deviations from a constant sound speed can lead to a noticeably different interference fringe placement and shape, and consequently to the inferred source-detector geometry. Further, comparisons of model calculations to experimentally observed fringe systems demonstrate the inadequacy of the constant sound speed model, whereas the use of the simple segmented profile is capable of replicating the observed patterns.